

RESEARCH ARTICLE

The impact of local soil class on the seismic behavior of a high-rise RC building

Kamran Samadi¹, Baris Gunes², Baris Sayin^{2*}

- ¹ Istanbul University-Cerrahpasa, Institute of Graduate Sciences, Istanbul, Türkiye
- ² Istanbul University-Cerrahpasa, Department of Civil Engineering, Istanbul, Türkiye

Article History

Received 28 May 2025 Accepted 10 July 2025

Keywords

Modal response spectrum analysis Soil class High-rise RC buildings Dual structural system

Abstract

This study numerically examines the impact of different soil classes on the seismic behavior of a high-rise RC building. For this purpose, a symmetric-plan, 30-story building model with reinforced concrete (RC) shear walls was prepared. The structural system of the model included two E-shaped core shear walls connected with coupling beams, forming a dual structural system consisting of core shear walls and a moment-resisting RC frame. Subsequently, earthquake parameters were obtained considering two different soil classes. Finally, modal response spectrum analysis was conducted considering two different response behaviors corresponding to upper (tower) and lower (podium) sections to determine the seismic performance level based on Turkish Building Earthquake Code (TBEC) 2018 conditions. Consequently, the relationship between soil class and seismic effects on the structural behavior of a high-rise building was established through a finite element model. The comparison of analysis results indicates that when transitioning from the ZB to the ZC local soil class, the maximum increase in axial load occurred in the corner columns, while the greatest increases in shear force were observed in the link beams and frame beams. Additionally, the highest shear force increases in the outer facade beams were also noted. Moreover, the bending moment transferred to the core shear walls nearly doubled, with the maximum bending moments in the core walls occurring at the transfer floor.

1. Introduction

According to the design spectrum approach, the soil effect is an important factor for high-rise buildings, since the seismic response in high-rise buildings increases at a higher rate when transitioning from hard soil to soft soil. Large displacements lead to a more extensive seismic design, which requires more complex and intensive calculation controls and higher costs. In addition, since tall buildings have longer periods, there may be a risk of resonance if they are built on soft soils.

Many studies investigated the effect of local soil on the seismic response of reinforced concrete (RC) buildings. However, most of these studies have investigated low- and mid-rise buildings. Existing studies in the literature are discussed under three categories: Low- and mid-rise buildings, multi-story buildings that are not classified as high-rise buildings, and high-rise RC buildings.

eISSN 2630-5763 © 2025 Authors. Publishing services by golden light publishing®.

^{*} Corresponding author (<u>barsayin@iuc.edu.tr</u>)

Studies investigating low- and mid-rise buildings have analyzed building models under different local soil classes to explore the relationship between soil type and seismic response. In these studies, Equivalent Lateral Force, Modal Response Spectrum, Nonlinear Time History, Nonlinear Pushover, and Incremental Dynamic Analysis (IDA) methods were used to assess seismic behavior of building models considering base shear, story displacement, lateral drift, period, story shear force, maximum moment, reinforcement bar (rebar) area, column demand-to-capacity ratios, mode shapes, moment-rotation curves, axial force, and acceleration parameters. Additionally, some studies examined the effects of other factors such as irregularities, the presence and location of shear walls, soil-structure interaction, seismic hazard levels, and the influence of different load combinations in addition to the effect of soil class. In general, studies have reported that the seismic response of building models increases as the local soil class changes from hard to soft [1-29]. In one such study, Yassin and Resatoglu [3] modeled an RC building with three different numbers of stories (4, 8, and 12) using both structural systems with and without shear walls, and an additional model of the 12-story building with irregularities in the shear wall system. Using the nonlinear pushover analysis, they compared base shear forces and displacements on medium and soft soils. Their results revealed that models with shear walls exhibited better seismic performance. Navarro et al. [4] measured the periods of 2to 9-story RC buildings using the Fourier spectrum method for different soil classes. The authors examined the relationship between the soil period and building period and pointed out that the local soil class affects earthquake damage and its distribution in the structural system. Tanijaya and Kwandou [5] applied modal response spectrum to 5-, 8-, and 10-story RC buildings and obtained parameters such as S_{DS} (Short period design spectral acceleration coefficient) and S_{D1} (Design spectral acceleration coefficient for 1.0 second period), displacement, shear force, maximum moment and rebar section, column demand capacity for hard, medium, and soft soils. Their results showed that the examined parameters changed depending on the soil conditions. Elsadany et al. [6] modeled 6-, 7-, and 10-story RC buildings as regular and irregular configurations and performed nonlinear pushover analysis. They investigated parameters such as mode shape, pushover curves, base shear force, displacement, period, irregularity effect, seismic vulnerability, and the response parameter R (Response Modification Factor) for medium and soft soils. Their findings revealed that the response parameter R increases as the soil conditions decrease. Avoil et al. [9] modeled an 8-story RC building and measured displacements using nonlinear pushover analysis in four different local soil classes. Their results showed that the displacements increased in parallel with the deterioration of the soil conditions. Ozmen and Tarakcı [10] investigated the effects of local soil conditions and foundation types on 25 different 4-story RC buildings using nonlinear pushover analysis. They examined the variations in parameters such as period, foundation size, soil stiffness, and lateral stiffness, and reported that the lateral stiffness and hinge distribution are not directly related to local soil conditions or foundation type, but rather the foundation is associated with the shear force. Javalekshmi and Chinmayi [11] investigated the effect of the location of the shear wall on four different local soil classes by analyzing 4 RC buildings of different story numbers with and without shear walls using time-history analysis. The parameters of base shear force, axial load, column bending moment, and shear force indicated that constructing the shear wall at the center of the plan (as a core shear wall) was the best option. Dhakal and Chaulagain [13] investigated a 9-story RC building with regular/irregular plan and hard, medium, and soft soil scenarios by modal response spectrum, considering the structure-soil relationship. Their results showed that as the soil conditions deteriorate, the displacement and inter-story drifts increase, and in terms of the structure-soil relationship, the base shear force decreases and the period of the structure increases.

In the second category of studies, low-rise and mid-rise building models with different frame types were addressed [30, 31]. For example, Galal and Naimi [32] modeled two RC structures with 6 and 20 stories and measured the story displacement, drift, and shear forces for different local soil classes (rock, stiff, medium,

soft) using time history analysis. Their results showed that the structure-soil interaction is more effective in the transition from hard to soft soil in a near-fault earthquake.

In the literature, only a limited number of studies have focused on high-rise RC buildings. Pahwa et al. [33] modeled a 30-story RC building and investigated the effect of local soil conditions (hard, medium, and soft) for both shear wall and non-shear wall configurations. Additionally, they prepared models where the shear wall thickness was uniform at 25 cm throughout, and models where it gradually reduced from 25 cm to 20 cm and 15 cm. Using the equivalent lateral force procedure, they evaluated the drift parameter for two types of models in a region with high seismicity. Their results showed that for both types of shear wall configurations, drift control was effective up to three-quarters of the building height. Surprisingly, the shear wall with varying thicknesses demonstrated better seismic performance. When transitioning from hard to soft soil, the role of the shear wall in drift control decreased compared to the frame system. Nevertheless, the shear wall still exhibited successful performance even on soft soil. In a similar study, Hosseini and Rao [34] modeled a 30-story RC building with different core shear wall configurations and investigated the effect of local soil (hard, medium, and soft). They measured various response parameters using the modal response spectrum under different load combinations. Their results showed that the box-shaped core shear wall has the best seismic performance in terms of maximum story displacement, period, and mode shape parameters. By examining various parameters such as the shape and location of the core shear wall, as well as local soil type are directly related to the displacements observed in the model. They observed an increase in axial load and moment in the columns during the transition from hard to soft soil. Consequently, the authors emphasized the importance of considering the structure-soil effect in high-rise reinforced concrete buildings.

This study investigated the relationship between building height, local soil class, and seismic risk level. A 30-story building model, with 3 of the floors defined as podium levels, was prepared. Accordingly, a high-rise building model appropriate to the scope and objectives of the study was used. In the model, the podium architecturally represents the parking area, while structurally enabling the development of more realistic and practical models by resisting the overturning moment. In the dual structural system consisting of core shear walls and coupling beams, two E-shaped shear walls with gradually varying thickness are used together with three coupling beams on each floor. Structural system moment and coupling ratio coefficient checks were performed to prepare a practical and scientifically correct model. Thus, the local soil class effect was analyzed using a model accurate for architectural and structural needs. Put simply, a finite element model was designed based on Turkish Building Earthquake Code (TBEC) 2018 [36] conditions, and subsequently, the local soil class effect was analyzed on an element basis (through internal forces) using a verified model.

2. Materials and methods

2.1. The examined building

To investigate the design-related seismic performance of a high-rise building, a 30-story building model was created using the ETABS [35] finite element software. The ETABS software, through its document feature, facilitates modeling, analysis, and interpretation of results for engineers and researchers. Furthermore, as a finite element analysis tool, ETABS enables the implementation of the seismic design requirements defined in the TBEC-2018 during both the analysis and design stages. For these reasons, it was selected for use in the modeling and analysis in this study.

In this model, three podium stories were designed above the foundation. Although podium stories are not mandatory in high-rise buildings, they provide a significant advantage by increasing the building's resistance against the overturning moment caused by earthquake-induced horizontal loads. The stories in the podium section were surrounded by basement shear walls on all four sides and were designated as parking areas. In other words, dead and live loads on these floors were estimated based on parking usage. The height of the

podium stories was 3.2 meters, and as shown in Fig. 1, the axis system consisted of five axes spaced at 8 meters in both the x and y directions. The length of the podium in both directions was 40 meters. The tower section of the model consisted of 27 stories, each with a story height of 3.2 meters. As shown in Fig. 1, the tower had a square and symmetrical floor plan. The total height of the building was 96 meters, and, considering the soil parameters, it was classified as a high-rise building.

The vertical load-bearing system of the model consists of square RC columns, RC beams, and slabs. The horizontal load-bearing system was designed as a structural system consisting of highly ductile RC shear walls and highly ductile moment-transmitting RC frames. Two E-shaped RC shear walls were added to the center of the building. These shear walls were connected with coupling beams to form the core shear walls of the model, which work together to resist seismic forces. The horizontal load-bearing system was designed as RC shear walls with openings in the x direction, connected by tie beams. Accordingly, the response modification factor (R) of the structural system was taken as 8. In the v direction, R was taken as 6 due to the solid RC shear walls. In the related literature and seismic codes, the role of resisting horizontal loads is shared between the RC shear core and the RC frame system, which is accepted for certain building heights. Typically, 75% of the earthquake effects are resisted by the RC shear core, while the remaining 25% is expected to be resisted by the RC frame system. This assumption was based on Article 4.3.4.5 of the TBEC-2018 which states: "In buildings where high-ductility reinforced concrete walls -either coupled (with link beams) or uncoupled, cast-in-place or precast- are used together with moment-resisting frames of high ductility level, or in combination with steel braced frames (concentric, eccentric, or buckling-restrained), the total overturning moment at the base resisted by the walls or braced frames shall not be less than 40% and not more than 75% of the total design seismic overturning moment for the entire building." [36]. Clause 12.2.5.1 of ASCE 7-22 states that "For a dual system, the moment frames shall be capable of resisting at least 25% of the design seismic forces. The total seismic force resistance is to be provided by the combination of the moment frames and the shear walls or braced frames in proportion to their rigidities." [41]. Since the structural model used in this study consists of RC moment-resisting frames and a core wall system (including shear walls and coupling beams), it qualifies as a dual system and therefore must be designed and evaluated in accordance with this design philosophy. The 3D views of the model are given in Fig. 2.

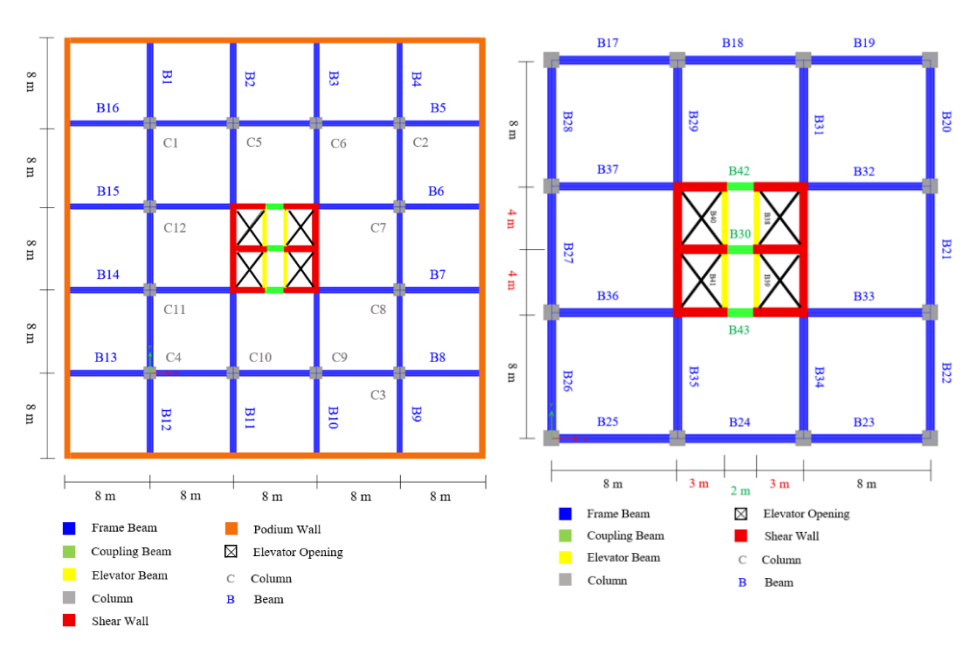


Fig. 1. Floor plan of the building model. Podium floors (left), typical floors (right)

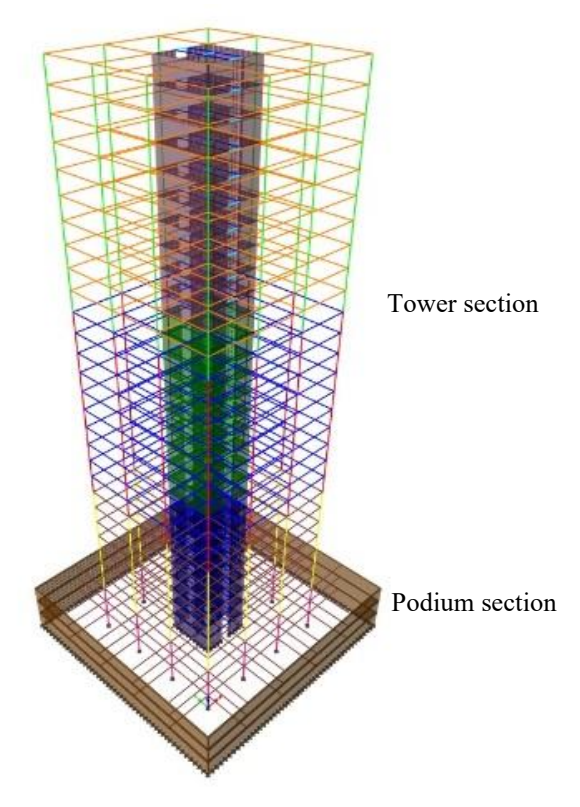


Fig. 2. 3D views of the building model

2.2. Material characteristics

In the building model, C50/60 class concrete was defined, and other material properties were determined according to TS500 [37]. Due to the restriction that only S420 and S500 grade steel is allowed for RC structural members of high-rise buildings, concrete steel was chosen as S420. Table 1 shows the characteristics of concrete and rebars defined in the model.

Table 1. Material characteristics of concrete and steel

Description	Concrete	Steel
Axial Compressive Strength, fck	50 MPa	
Modulus of Elasticity, Ec and Es	36981 MPa	$2\times10^5\mathrm{MPa}$
Axial Tensile Strength, fctk	2.48 MPa	
Poisson's Ratio, μ _c	0.20	
Shear Modulus, Gej	14792 MPa	
Coefficient of Thermal Expansion, α_t	10^{-5} / C°	12^{-6} /C $^{\circ}$
Partial Safety Factor for Material, γ_{mc} , γ_{ms}	1.50	1.15
Design Compressive Strength, fcd	33.33	
Design Axial Tensile Strength, fctd	1.65	
Unit Weight	$2500~kg/m^3$	7850 kg/m^3
Characteristic Yield Strength, $f_{yk} = R_e$		420 MPa
Design Yield Strength, fyd		365 MPa

2.3. Design loads

2.3.1. Vertical static loads

Vertical static load calculations in high-rise buildings are determined according to the building's intended use, structural system, slab system, and façade design. The determined dead and live loads are presented in Table 2 [38].

Deal loads $(w_{G,j}^{(S)})$ and live loads $(w_{Q,j}^{(S)})$ were combined using Eq. 1. Since the intended use of the building is residential, the n coefficient was taken as 0.3. Snow load was taken as 0.75 kN/m² depending on the height and location of the building.

$$w_{G,i}^{(S)} + nw_{O,i}^{(S)} \tag{1}$$

2.3.2. Earthquake and wind loads

In the calculation of seismic parameters, the spectral acceleration coefficients S_s and S_l were obtained from the interactive web application of the Turkish Disaster and Emergency Management Presidency (AFAD) [39], based on the location of the structure for each level of seismic ground motion. These values are presented in Table 3. Subsequently, lateral and vertical elastic design spectra were obtained for each of the four earthquake ground motion levels. The spectra are presented in Fig. 3. The wind load analysis for the model was performed according to the description provided in the local code, TS498 [38].

2.3.3. Lateral earth pressure

Lateral earth pressure was calculated as the sum of two components: static earth pressure and additional earth pressure induced by seismic effects. Static Earth Pressure was calculated based on the cohesion of the soil according to the TBEC-2018 [36] and was calculated using Eq. 2, assuming that the soil is cohesionless. Additional earth pressure induced by seismic effects was calculated using Eq. 3.

$$P = 0.2 (\gamma \times H_b + q)$$

$$P = 0.2 (18 \times 9.6 + 0) = 34.6 \text{ kN/m}^3$$

$$\Delta p = 0.4 \text{ S}_{DS} \gamma H_b$$

$$\Delta p = 0.4 \times 1.0248 \times 18 \times 9.6 = 70.8 \text{ kN/m}^3$$

$$H = P + \Delta p = 105.4 \text{ kN/m}^3$$
(3)

Table 2. Dead and live loads

Dead loads	Live loads		
Description	Value (kN/m²)	Story	Value (kN/m²)
Finishing Load (Residential)	2	Typical Floors (Residential)	2
Finishing Load (Parking Garage)	1	Podium Floors (Parking Garage)	5
Finishing Load (Roof)	5	Roof Floor	1.5
Partition Wall Load (not present in the garage)	1.5		

Table 3. Seismic parameters considered in the analyses

Earthquake ground motion level	Period (year)	S_s	S ₁
DD-1	2475	1.496g	0.416g
DD-2	475	0.854g	0.238g
DD-3	72	0.342g	0.097g
DD-4	43	0.228g	0.064g

DD-1: Earthquake ground motion level with a probability of being exceeded in 50 years of 2%

DD-2: Earthquake ground motion level with a probability of being exceeded in 50 years of 10%

DD-3: Earthquake ground motion level with a probability of being exceeded in 50 years of 50%

DD-4: Earthquake ground motion level with a probability of being exceeded in 50 years of 68%

2.4. Determination of analysis parameters

The horizontal seismic load in the x-direction is carried by columns, beams, coupling beams, and hollow shear walls, while in the y-direction, it is carried by columns, beams, and solid shear walls. However, Eqs. 4-6 are used to analyze the upper and lower parts of high-rise buildings with different *R* factors. Using both equations, the *R* factors for the x and y directions were calculated for the upper and lower parts of the model. Accordingly, the structural response modification factor (*R*) for the upper part (tower) of the model was calculated as 8 in the x direction and 7 in the y direction. It was calculated as 2.5 in both directions of the lower (podium) part. The *R* factor, commonly referred to in the literature as the response modification factor, is used to reduce the earthquake loads and is entirely dependent on the structural system [41]. The linear analysis parameters and method are presented in Table 4.

 $\vartheta^{(X)}_{lower} = \left(1 - \vartheta^{(X)}_{upper}\right) \frac{(R_a)_{upper}}{(R_a)_{lower}}$

$$(R_{a})_{upper} = \frac{R_{upper}}{I}, \quad T_{p} > T_{B}$$

$$(R_{a})_{upper} = D_{upper} + \left(\frac{R_{upper}}{I} - D_{upper}\right) \frac{T_{p}}{T_{B}}, \quad T_{p} \leq T_{B}$$

$$T_{p}^{(X)} = 3.64 > T_{B} = 0.3484 \qquad (R_{a})_{upper}^{(X)} = \frac{8}{1} = 8$$

$$T_{p}^{(Y)} = 3.15 > T_{B} = 0.3484 \qquad (R_{a})_{upper}^{(Y)} = \frac{7}{1} = 7$$

$$(R_{a})_{lower}^{(X)} = \frac{(R_{a})_{upper}^{(X)}}{\vartheta^{(X)}}$$

$$\vartheta^{(X)} = \vartheta^{(X)}_{upper} + \vartheta^{(X)}_{lower}$$

$$\vartheta^{(X)}_{upper} = \frac{V_{x,upper}^{(X)}}{V_{x,all}^{(X)}}$$
(5)

$$(R_a)_{lower}^{(Y)} = \frac{(R_a)_{upper}^{(Y)}}{\vartheta^{(X)}}$$

$$\vartheta^{(Y)} = \vartheta^{(Y)}_{upper} + \vartheta^{(Y)}_{lower}$$
(6)

$$\vartheta^{(Y)}_{upper} = \frac{V_{x,upper}^{(Y)}}{V_{x,all}^{(X)}}$$

$$\vartheta^{(Y)}_{lower} = \left(1 - \vartheta^{(Y)}_{upper}\right) \frac{(R_a)_{upper}}{(R_a)_{lower}}$$

$$(R_a)_{lower}^{(X)} = 2.635, \qquad (R_a)_{lower}^{(Y)} = 2.625$$

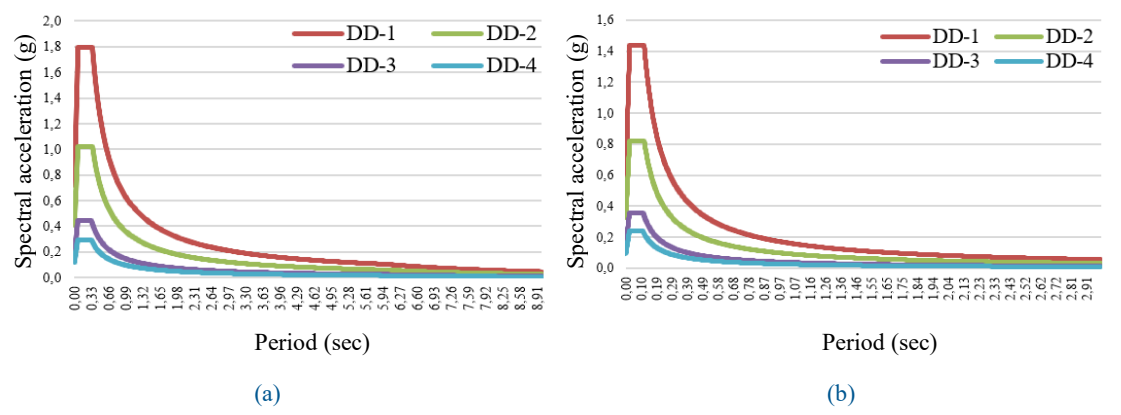


Fig. 3. Design spectra: (a) Lateral, (b) Vertical

Table 4. Parameters used in the analyses

Parameter	Value / Class
Building Use Class, BUC	3
Building Importance Factor, I	1.0
Earthquake Design Class, EDC	1
Building Height Class, BHC	1
Structural Design Targets	Controlled Damage for DD-2
Design/Assessment Method	Design Based on Strength Response Spectrum Analysis
Response Modification Factor, R	x direction: $(R_a)_{upper} = 8$; $(R_a)_{lower} \simeq 2.5$ y direction: $(R_a)_{upper} = 7$; $(R_a)_{lower} \simeq 2.5$
Overstrength Factor, D	2.5
Local Soil Class	ZC

Table 5. Period values and mass participation ratios

Mod	Dania	Mass participation ratio			ntio	
	renoc	d (sec)	x y			У
	A	В	A	В	A	В
1	3.364	3.364	55%	72%	0	0
2	3.152	3.152	0	0	52%	69%

Scenario A: All stories are considered.

Scenario B: Podium stories are not considered.

Since the lower three stories of the building constitute the podium section, it was necessary to verify whether the total building height should be measured from the foundation level or the top of the podium. As the podium stories were enclosed on all four sides by rigid basement shear walls, the model was analyzed for two different heights. As seen from the resulting periods presented in Table 5, both analyses yielded identical period values satisfying the condition, $T_{p,all} \le 1.1 \ T_{p,upper}$. Therefore, the total building height was taken as $H_N = 86.4$ m in seismic analyses.

2.5. Modal response spectrum analysis

In this study, the design of high-rise reinforced concrete buildings was based on the theoretical framework of the local code TBEC-2018. The TBEC-2018 outlines a three-stage design approach for tall buildings. Stage I (Preliminary Design) and Stage II (Performance Evaluation for an Alternative Performance Objective) are both addressed through linear analysis, as this method is widely accepted in the literature for preliminary design and initial sizing. However, since structural performance under seismic action is expected to include characteristics such as stiffness, strength, and ductility, Stage III of TBEC-2018 also incorporates nonlinear time-history analysis to account for the inelastic deformation capacity of structural members during earthquakes. As this study is limited to preliminary design and sizing, linear analysis was employed, including the assessment of the effects of local soil class.

In this method, the seismic design spectrum corresponding to a given earthquake direction is used to calculate the peak response values in each vibration mode using modal analysis. The peak modal responses, which are calculated for a sufficient number of vibration modes but are not simultaneous, are then statistically combined to estimate the approximate maximum responses. However, the results of the modal response spectrum must be revised to satisfy the minimum base shear force required by the equivalent lateral force procedure. Initially, the model was analyzed using the modal response spectrum, considering two different *R* factors for the upper (tower) and lower (podium) parts to evaluate whether the Controlled Damage performance level was satisfied under the DD-2 earthquake ground motion. The linear design of the model was first analyzed for local soil class ZC, and then the same design steps were repeated for local soil class ZB. Thus, the influence of the local soil class at the structural element level was demonstrated. To establish a realistic relationship between local soil classes and seismic hazard levels for these two soil types, real locations and soil parameters were selected from Istanbul province. As shown in Fig. 4, the selected locations mostly have local soil classes of ZB and ZC. Descriptions of the ZB and ZC soil classes are provided in Table 6. In Fig. 5, the Elastic Design Spectra corresponding to the DD-2 earthquake ground motion level are comparatively presented for the locations associated with ZB and ZC local soil classes.

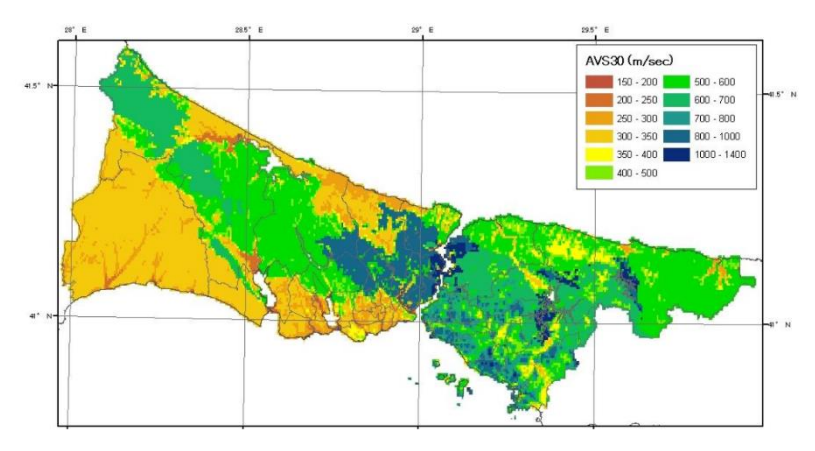


Fig. 4. Average (V_S)₃₀ distribution map of Istanbul [40]

Table 6	Characteristic	es of the 2	ZB and ZC	Soil Classes

Local soil class	Soil class	(Vs)30
ZB	Slightly weathered, moderately strong rock formations	760 - 1500
ZC	Very dense sand, gravel, and stiff clay layers, or highly weathered, heavily fractured, weak rock	360 – 760

(V_S)₃₀: Average shear wave velocity in the upper 30 meters [m/s]

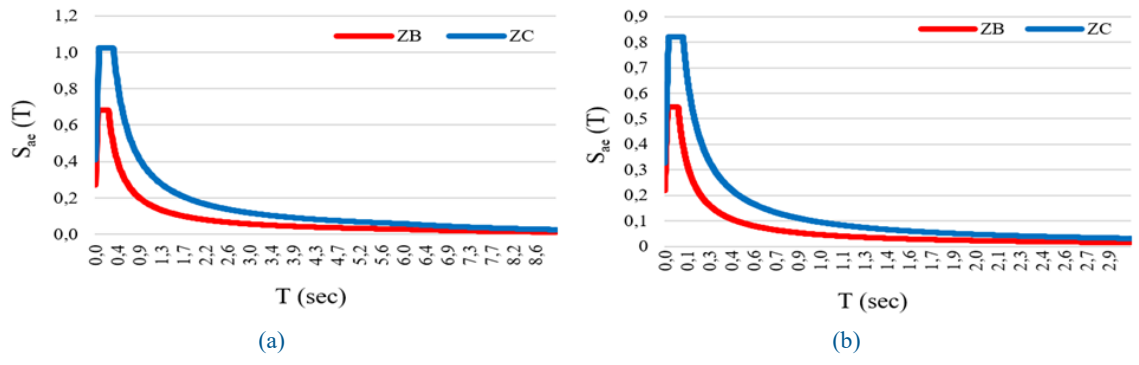


Fig. 5. Design spectra for ZB and ZC local soil classes; (a) Lateral, (b) Vertical

According to the TBEC-2018 [36], beams and columns were modeled using bar elements. At the beam and column joints, all six degrees of freedom were defined in the model. Since the structural layout is symmetrical, floor slabs were modeled as rigid diaphragms. The same modeling approach was applied to the transfer floor slabs. Shear walls were modeled using shell elements, which include degrees of freedom for both in-plane and out-of-plane displacements. At the joints of these elements, all six degrees of freedom were defined. Coupling beams were modeled using bar elements. The basement shear walls were also modeled using shell elements, with all six degrees of freedom defined at their connecting nodes. At the base of the model, the lower ends of the vertical elements (columns and shear walls) were modeled as fixed supports. Table 7 presents the effective section stiffness values defined for the RC members. A 5% damping ratio was used in the elastic design spectrum corresponding to the DD-2 as specified in the seismic code.

Table 7. Effective section stiffness factors

Structural Member	Effective Section	Stiffness Factor
Shear – Slab (In-plane)	Axial	Shear
Shear Wall	0.50	0.50
Basement Shear	0.80	0.50
Slab	0.25	0.25
Shear – Slab (Out-of-plane)	Flexural	Shear
Shear Wall	0.25	1.00
Basement Shear	0.50	1.00
Slab	0.25	1.00
Rod Element	Flexural	Shear
Coupling Beam	0.15	1.00
Frame Beam	0.35	1.00
Frame Column	0.70	1.00
Shear Wall (Equivalent Strut)	0.50	0.50

2.6. Load combinations

To combine the effects of seismic loads with other vertical and lateral dead-live loads, two main load combinations were employed. In these combinations, the parameter H represents the lateral earth pressure and was applied to the podium portion of the model (basement frame levels). The parameter $E_d^{(H)}$ denotes the lateral seismic effect and was calculated using Eq. 7. Additional eccentricity effects in both the x and y directions were also incorporated into the model. The seismic design eccentricity was considered as $\pm 5\%$ of the story height perpendicular to the direction of the seismic load. Accordingly, for each $E_d^{(X)}$ and $E_d^{(Y)}$ component, three variations were applied: (a) without additional eccentricity, (b) with +0.05 eccentricity, and (c) with -0.05 eccentricity. Consequently, a total of 144 load combinations were defined for both the upper (tower) and lower (podium) parts of the structure under the two main load combinations.

$$G + Q + 0.2S + E_{d}^{(H)} + 0.3E_{d}^{(Z)}$$

$$0.9G + H + E_{d}^{(H)} - 0.3E_{d}^{(Z)}$$

$$E_{d}^{(H)} = \mp E_{d}^{(X)} \mp 0.3 E_{d}^{(Y)}$$

$$E_{d}^{(H)} = \mp E_{d}^{(Y)} \mp 0.3 E_{d}^{(X)}$$
(7)

To combine the effects of wind loads in combination with other dead-live loads, two additional load combinations expressed in Eq. 8 were defined in the model based on the TS500 [37] standard. Here, the parameter W represents the wind load, which was applied in both the x and y directions as positive (from the right) and negative (from the left). Accordingly, four load combinations were generated for each direction, resulting in a total of eight wind load combinations implemented in the structural model.

$$1.0G + 1.3Q \mp 1.3W$$

$$0.9G \mp 1.3W$$
(8)

3. Results and discussion

3.1. Modal analysis results

Table 8 presents the mass participation ratios. In the modal analysis, vibration modes in both the X and Y directions were included until at least 95% of the total building mass was achieved [36]. The number of modes was determined accordingly. Table 9 presents the corresponding modal response results for the same mode shapes.

3.2. Moment control of the structural system

The lateral load-bearing system of the model must function through the combined action of RC frames (columns and beams) and shear walls. To ensure this behavior, the distribution ratio of earthquake loads among structural elements was limited using Eq. 9. In this equation, M_o represents the total overturning moment at the base of the entire building due to earthquake loads and M_{DEV} is the overturning moment at the base of the RC shear wall caused by earthquake loads.

The moments obtained by the equivalent lateral force procedure for the whole structural system and only for the shear walls of the building are presented in Table 10. According to the results, it was verified that the design satisfies the limitation condition stipulated in Eq. 9 in both axis directions.

$$0.40 M_o < \sum M_{DEV} < 0.75 M_o$$

$$\frac{M_{DEV}}{M_o} = \frac{M_3}{M_Y} = \frac{425789.3175}{802625.3679} = 0.5305 = 53$$

$$\frac{M_{DEV}}{M_o} = \frac{M_2}{M_X} = \frac{435600.663}{802625.368} = 0.5427 = 54\%$$

Table 8. Mass participation ratios

Mode	Period (sec)	UX	UY	UZ	SumUX	SumUY
1	3.364	0.5459	0	0	0.5459	0
2	3.152	0	0.5221	0	0.5459	0.5221
3	2.688	0	0	0	0.5459	0.5221
4	0.981	0.1197	0	0	0.6657	0.5221
5	0.884	0	0	0	0.6657	0.5221
6	0.752	0	0.1431	0	0.6657	0.6652
7	0.487	0.0433	0	0	0.709	0.6652
8	0.469	0	0	0	0.709	0.6652
9	0.317	0	0.0565	0	0.709	0.7217
10	0.302	0.0241	0	0	0.7331	0.7217
11	0.299	0	0	0	0.7331	0.7217
12	0.212	0	0	0	0.7331	0.7217
13	0.206	0.0169	0	0	0.75	0.7217
14	0.183	0	0.0313	0	0.75	0.753
15	0.162	0	0	0	0.75	0.753
16	0.151	0.0143	0	0	0.7643	0.753
17	0.13	0	0	0	0.7643	0.753
18	0.124	0	0.023	0	0.7643	0.7761
19	0.116	0.0133	0	0	0.7776	0.7761
20	0.108	0	0	0	0.7776	0.7761
21	0.093	0	0.0223	0	0.7776	0.7983
22	0.093	0.0148	0	0	0.7924	0.7983
23	0.092	0	0	0	0.7924	0.7983
24	0.08	0	0	0	0.7924	0.7983
25	0.077	0.0207	0	0	0.8131	0.7983
26	0.075	0	0.0253	0	0.8131	0.8237
27	0.07	0	0	0	0.8131	0.8237
28	0.065	0.0362	0	0	0.8493	0.8237
29	0.063	0	0.0365	0	0.8493	0.8602
30	0.063	0	0	0	0.8493	0.8602
31	0.058	0.0581	0	0	0.9073	0.8602
32	0.057	0	0	0	0.9073	0.8602
33	0.055	0	0.052	0	0.9073	0.9122

Table 8. Continued

M	ode	Period (sec)	UX	UY	UZ	SumUX	SumUY
3	34	0.052	0.0424	0	0	0.9497	0.9122
3	35	0.051	0	0	0	0.9497	0.9122
3	36	0.05	0	0.0362	0	0.9497	0.9483
3	37	0.047	0	0	0	0.9497	0.9483
3	38	0.047	0.0154	0	0	0.9652	0.9483
3	39	0.045	0	0.0158	0	0.9652	0.9641

Table 9. Modal periods and frequencies

Mode	Period (sec)	Frequency (cyc/sec)	CircFreq (rad/sec)	Eigenvalue (rad²/sec²)
1	3.364	0.297	1.8678	3.4888
2	3.152	0.317	1.9934	3.9737
3	2.688	0.372	2.3378	5.4652
4	0.981	1.019	6.4048	41.0218
5	0.884	1.132	7.1107	50.562
6	0.752	1.329	8.3506	69.7318
7	0.487	2.055	12.9123	166.7277
8	0.469	2.131	13.3926	179.3612
9	0.317	3.158	19.8442	393.7926
10	0.302	3.31	20.7982	432.5671
11	0.299	3.341	20.9935	440.7273
12	0.212	4.706	29.5714	874.468
13	0.206	4.843	30.4288	925.9123
14	0.183	5.476	34.4083	1183.928
15	0.162	6.189	38.8885	1512.3143
16	0.151	6.63	41.6573	1735.3323
17	0.13	7.671	48.2008	2323.3143
18	0.124	8.047	50.5627	2556.5876
19	0.116	8.613	54.1187	2928.8331
20	0.108	9.237	58.037	3368.2927
21	0.093	10.716	67.3322	4533.6318
22	0.093	10.772	67.6825	4580.9188
23	0.092	10.865	68.2674	4660.4438
24	0.08	12.495	78.5104	6163.8823
25	0.077	13.051	82.0028	6724.4642
26	0.075	13.288	83.4915	6970.8271
27	0.07	14.188	89.1485	7947.4571
28	0.065	15.282	96.0196	9219.7581
29	0.063	15.778	99.1353	9827.8115
30	0.063	15.896	99.8777	9975.5531
31	0.058	17.328	108.8777	11854.3562
32	0.057	17.685	111.118	12347.221

TO 1	1 .	1 (١.	\sim		1
Iа	h	le v) (l int	ntim	ned

Mode	Period (sec)	Frequency (cyc/sec)	CircFreq (rad/sec)	Eigenvalue (rad²/sec²)
33	0.055	18.023	113.2436	12824.1218
34	0.052	19.25	120.9498	14628.8565
35	0.051	19.505	122.5512	15018.7857
36	0.05	20.028	125.8374	15835.0548
37	0.047	21.301	133.8353	17911.882
38	0.047	21.443	134.7333	18153.0698
39	0.045	22.259	139.8592	19560.59

Table 10. All moments in the structural system

Load		A	В		
Loau	Mx	$M_{ m Y}$	M_2	M ₃	
EQX	0	-802625	-2.8E-05	425789	
EQX	-9.5E-06	-802625	-3.3E-05	425789	
EQX	1.0E-05	-802625	-2.3E-05	425789	
EQY	802625	0	435600.7	-2.9E-05	
EQY	802625	7.9E-07	435601	-3.0E-05	
EQY	802625	-1.4E-06	435601	-2.8E-05	

A: Moment acting on the whole structural system

B: Moment acting on the shear walls

3.3. Preliminary sizing of structural elements

The preliminary sizing of the columns was carried out using the equivalent lateral force procedure under axial loading conditions (1.4G + 1.6Q), without considering seismic effects. Accordingly, it was verified that the selected dimensions meet the conditions envisaged in TBEC-2018 [36] and TS500 [38]. The preliminary sizing of the core shear wall was performed under the G+Q+E load combination, in accordance with the minimum section requirements for RC shear walls with high ductility. In the preliminary sizing of the beams, RC beams with high ductility were considered. In the preliminary sizing of slabs, additional eccentricity effects in both earthquake directions (x and y) were taken into account, based on the rigid diaphragm assumption. The final dimensions of the structural elements are presented in Table 11.

3.4. Coupling ratio controls

The coupling ratio was calculated using Eq. 10, considering that the coupling ratio along the longitudinal direction of the coupled (perforated) core shear walls falls satisfies the required range of a minimum of 1/3 and a maximum of 2/3. In Equation 10, c denotes the distance between the centroids of the cross-sections of the coupled (slotted) wall segments, N_{v} represents the total axial tension and compression forces at the base of the wall segments caused by the shear forces developed in the coupling beams under seismic effects, and M_{1} , M_{2} refer to the bending moments at the base of the wall segments due to seismic action.

$$\Omega = \frac{c N_v}{M_{DEV}} = \frac{c N_v}{M_1 + M_2 + c N_v} \tag{10}$$

(11)

	Column	She	Shear wall			Beam			
Story	Section dimensions	Thickness (cm)	Cross-sectional area	Sectio	n dimensio	ons (cm)	(cm)		
	(cm)	Tillekiless (cili)	(cm^2)		B2*	В3*			
1 – 3	120×120	50	810	50×80		50×75			
4 - 10	100×100	30	810	30^80	30×60	30^73	20		
11 - 20	90×90	45	740	40×80	30^00	45×75	20		
21 – 30	80×80	40	660	40×70		40×75			

Table 11. Dimensions of the structural elements

The coupling ratio was calculated as 0.583 using Eq. 10. This value satisfies the requirement specified in TBEC-2018 [36]. Since the value is greater than 1/3, it confirms that the system behaves as a coupled shear wall in the x-direction. Additionally, since the ratio is less than 2/3, the condition to prevent excessive axial forces in the individual shear wall segments is also satisfied.

3.5. Modal response spectrum analysis results

The results obtained from modal response spectrum analysis were revised considering the minimum base shear forces in the equivalent lateral force procedure defined by Eq. 11 where m_t represents the total mass of the upper portion of the model above the podium floors. The parameter α_H is defined by Eq. 12. Since the total building height is $H_N = 86.4 \text{ m}$, α_H was taken as 1.

$$V_{t,min} = 0.04 \ \alpha_H \ m_t \ S_{DS} \ g \eqno(11)$$

$$\alpha_H = 1.0 \qquad \qquad H_N \ \leq 105 \ m$$

$$\alpha_H = 2.05 - 0.01 H_N \qquad \qquad 105 \ m < H_N \ \leq 155 \ m \eqno(12)$$

$$\alpha_H = 0.5 \qquad \qquad 155 \ m < H_N$$

Since different R factors were used for the upper section (tower) and lower section (podium) of the model, the minimum base shear force of the equivalent lateral force procedure was calculated separately for each section.

$$(V_{t,min})_{upper} = 8595 \text{ kN}$$

$$(V_{t,min})_{tower} = 11389 \text{ kN}$$

Table 12 shows the results of the equivalent lateral force procedure and modal response spectrum for the upper part of the model. According to the results, the base shear forces in the x and y directions obtained by the modal response spectrum are lower than those obtained by equivalent lateral force procedure and these values had to be increased according to Eq. 13. Using the amplification factors given in Eq. 13, the modal response spectrum analysis was repeated, and the revised results are presented in Table 13. For the lower portion of the model (three podium floors), the minimum base shear force $(V_{t,min})_{tower}$ was calculated as 11389 kN.

$$\beta_{tE}^{(X)} = \frac{V_{t,min}^{(X)}}{V_{tx}^{(X)}} \ge 1.0, \qquad \beta_{tE}^{(Y)} = \frac{V_{t,min}^{(Y)}}{V_{ty}^{(Y)}} \ge 1.0$$
 (13)

^{*} B1: Frame Beam, B2: Elevator Beam, B3: Coupling Beam

Table 12. Results for the upper section of the model								
Analysis Method	Axis	FX (kN)	FY (kN)	FZ (kN)	MX (kNm)	MY (kNm)	MZ (kNm)	
	EQX	-8460	0	0	0	-626182	101515	
	EQX	-8460	0	0	-8.2E-06	-626182	111666	
Equivalent lateral	EQX	-8460	0	0	8.6E-06	-626182	91363	
force	EQY	0	-8460	0	626182	0	-101515	
	EQY	0	-8460	0	626182	7.4E-07	-111666	
	EQY	0	-8460	0	626182	-1.2E-06	-91363	
Modal response spectrum analysis	EX (upper)	3643	0.0011	0	0.0115	179882	48084	
	EY (lower)	0.001	5272	0	223176	0.012	69584	

Table 12. Results for the upper section of the model

The results of the equivalent lateral force procedure and mode coupling analyses for the lower part of the model are given in Table 14. According to the results, the base shear forces in the x and y directions obtained by the modal response spectrum are lower than those obtained by the equivalent lateral force procedure. However, since the base shear forces obtained by modal response spectrum were greater than the minimum base shear force, the factors in the x and y directions were less than 1. Therefore, it was not necessary to revise the modal response spectrum results for the lower portion of the model.

3.6. Inter-story drift checks

Assuming that the infill walls are made of brittle materials, flexible joints exist between frame elements, façade elements are flexibly connected to exterior frames, or the infill walls are independent of the frame, the inter-story drifts of the model were limited according to the value calculated using Eq. 14. According to the mode coupling analyses, the inter-story drifts in both the x and y directions were found to be below the limits specified in the local code (Fig. 6).

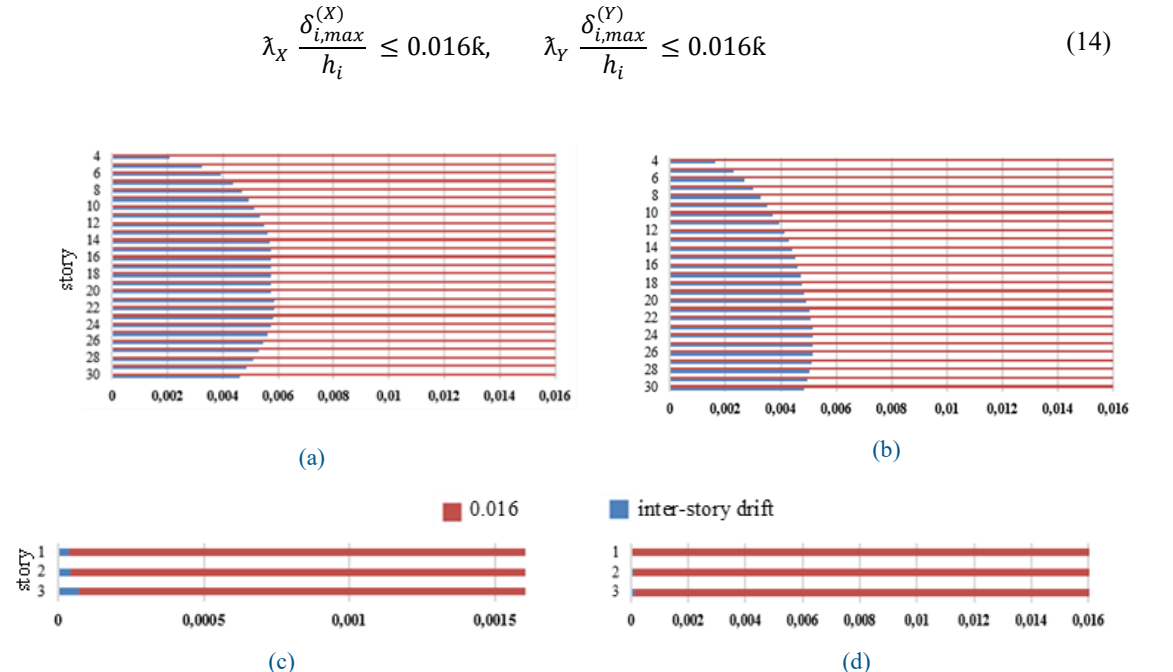


Fig. 6. Inter-story drift values: (a) x-upper portion, (b) y-upper portion, (c) x-lower portion, (d) y-lower portion

Analysis method	Axis	Fx (kN)	Fy (kN)	Fz (kN)	Mx (kNm)	My (kNm)	Mz (kNm)
Modal response	EX (upper)	8595	0.0011	0	0.0272	424432	113453
spectrum analysis	EY (lower)	0.001	8595	0	363875	0.0194	113453

Table 14. Results for the lower section of the model

Analysis method	Axis	Fx (kN)	Fy (kN)	Fz (kN)	Mx (kNm)	My (kNm)	Mz (kNm)
	EQX	-29403	0	0	0	-216892	352837
	EQX	-29403	0	0	0	-216892	411644
Equivalent lateral	EQX	-29403	0	0	0	-216892	294031
force	EQY	0	-29403	0	216892	0	-352837
	EQY	0	-29403	0	216892	0	-411644
	EQY	0	-29403	0	216892	0	-294031
Modal response spectrum analysis	EX (upper)	19840	0.0711	0	0.3838	589691	267779
	EY (lower)	0.042	21736	0	640685	0.2845	291542

3.7. Torsional irregularity checks

To evaluate torsional irregularity, a Torsional Irregularity Coefficient was defined and limited using Eq. 15, considering the effect of $\pm 5\%$ accidental eccentricity in the inter-story drift calculations. As shown in Fig. 7, all calculated values remained below the limit of 1.2. Therefore, it was concluded that the model has no torsional irregularity in either the x or y directions.

$$\eta_{bi} = \frac{\left(\Delta_i^{(X)}\right)_{max}}{\left(\Delta_i^{(X)}\right)_{ort}} \le 1.2$$
(15)

3.8. Linear design results

The mode coupling analyses were performed for structural element designing by evaluating whether the model satisfies the Controlled Damage performance level under the DD-2 earthquake ground motion, considering two different *R* factors for the upper (tower) and lower (podium) parts of the structure.

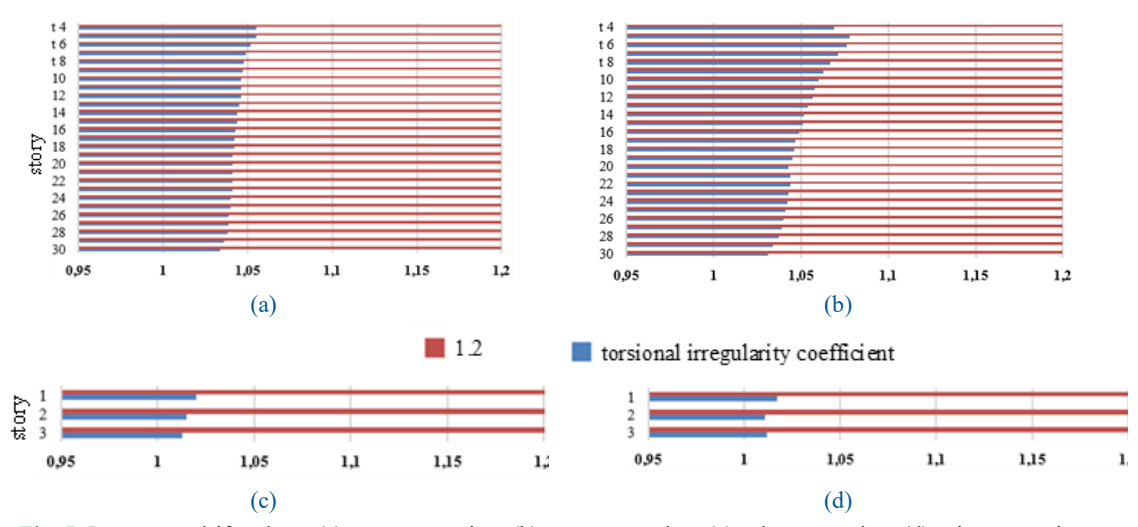


Fig. 7. Inter-story drift values: (a) x-upper portion, (b) y-upper portion, (c) x-lower portion, (d) y-lower portion

3.8.1. Column design

Based on the results of the modal response spectrum, the section adequacy of the columns was checked under seismic effects by ensuring compliance with the condition given in Eq. 16. In addition, upward live load reduction was applied in accordance with TS498 [38]. The final design properties of the column sections are given in Table 15.

$$N_{dm} = G + Q + E \le 0.4 f_{ck} A_c$$
 (16)

3.8.2. Beam design

Using the results of the modal response spectrum, longitudinal rebar and stirrup design for beams were carried out. As illustrated in Fig. 8, three types of beam elements were defined in the model. This arrangement was applied up to the top floor, including the tower portion of the structure. Table 16 shows the final design specifications for the beam cross-sections. For all frame beams, stirrups were selected as $4\phi 8/10$ in confinement regions and $4\phi 8/20$ in mid-span regions.

Table 15. Column cross-section dimensions and rebar areas

Story	ory Column Load com		Rebar		nber of rrups	Stirrup — diameter (mm)	s (mm)	
	section (cm)		quantity/arameter	X	у	diameter (mm)		
1 – 3	120×120	G + Q + E	32φ26	7	7	14	100/150	
4 - 10	100×100	G + 0.95Q + E	24φ26	6	6	14	100/150	
11 - 20	90×90	G + 0.6Q + E	24φ26	5	5	14	100/150	
21 - 30	80×80	G + 0.6Q + E	20φ26	4	4	12	100/150	

Table 16. Longitudinal rebar layout in beams

True	Top longitudinal rebar		Wah nahan	
Type	Dimensions (cm)	Bottom longitudinal rebar	Web rebar	
	50~90	$6\phi 18 + 2\phi 14$	2×2112 / 250	
Α	30^80	$4\phi 18 + 2\phi 16$	2×2φ12 / 250	
D	50×80	$4\phi 18 + 2\phi 16$	2×2φ12 / 250	
Ь	30^80	$4\phi 18 + 2\phi 16$	2^2ψ12 / 230	
٨	50×80	$6\phi 22 + 3\phi 14$	2×2φ12 / 250	
А	30^80	$4\phi 18 + 2\phi 16$	2^2ψ12 / 230	
D	50×80	$6\phi 18 + 3\phi 16$	2×2φ12 / 250	
D	30^80	$4\phi 18 + 2\phi 16$	2^2ψ12 / 230	
A 40×80		$6\phi 22 + 3\phi 14$	2×2φ10 / 250	
А	40^60	$5\phi 16 + 2\phi 14$	2^2ψ10 / 230	
R	40×80	6φ22	2×2φ12 / 250	
ь	40^00	$4\phi 16 + 2\phi 14$	2^2ψ12 / 23 0	
٨	40×70	$6\phi 22 + 3\phi 12$	2×2φ12 / 250	
Α	40^/0	$5\phi 16 + 2\phi 14$	2^2ψ12 / 230	
21–30	40×70	6φ22	2×2φ12 / 250	
ь	40^/0	$4\phi 16 + 2\phi 14$		
C	30×60	4φ14	2φ12 / 250	
	30.00	4φ14	2ψ12 / 230	
	Type A B A B A C	A 50×80 B 50×80 A 50×80 B 50×80 A 40×80 A 40×80 A 40×70 B 40×70	Type Dimensions (cm) A 50×80 6φ18 + 2φ14 B 50×80 4φ18 + 2φ16 A 50×80 4φ18 + 2φ16 A 50×80 6φ22 + 3φ14 B 50×80 6φ18 + 3φ16 A 40×80 6φ22 + 3φ14 B 40×80 6φ22 + 3φ14 B 40×80 6φ22 A 40×70 6φ22 + 3φ12 B 40×70 5φ16 + 2φ14 B 40×70 6φ22 4φ16 + 2φ14 6φ22 4φ16 + 2φ14 4φ16 + 2φ14 C 30×60	

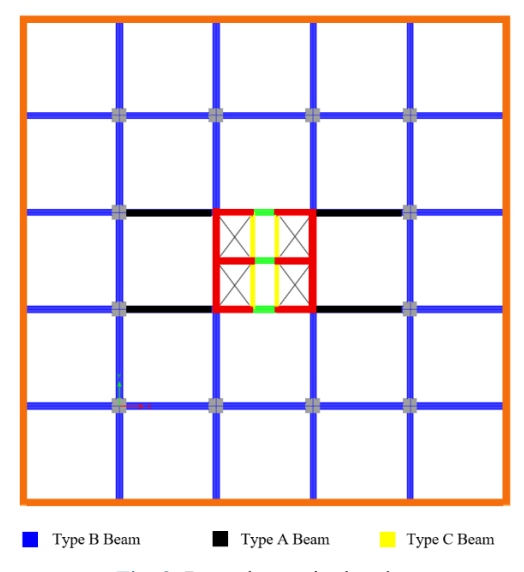


Fig. 8. Beam layout in the plan

3.8.3. Shear wall design

Using the results of the modal response spectrum, rebar calculations were performed separately for the region within and above the critical wall height, as well as for the boundary zones adjacent to the columns. The types and quantities of rebars were determined accordingly. Tables 17 and 18 show the calculated vertical and lateral rebars for the shear walls.

Table 17. Shear wall web rebars

Story	Shear thickness		Lateral rebar			
•	(mm)	Within the criti	cal shear height	Outside critica	al shear height	_
		Short Face	Long Face	Short Face	Long Face	
1-10	500	7φ12	32φ12	7φ12	40φ12	φ14 / 150
11-20	450	-	-	6φ12	42φ12	φ14 / 200
21-30	400	-	-	6φ12	44φ12	φ14 / 250

Note: In the E-shaped shear wall configuration, the "long face" refers to the vertical spine of the "E", while the "short faces" correspond to the horizontal arms.

Table 18. Shear wall boundary zone rebars

			Vertical rebar				Lateral rebar			
Story	Shear thickness (mm)	Within the critical shear height				Within the critical shear height		Outside critical shear height		
	,	Short Face	Long Face	Short Face	Long Face	Short Face	Long Face	Short Face	Long Face	
1–10	500	16φ20	26φ20	16φ20	16φ20	5 pcs \phi14	6 pcs \$14	2 pcs \phi12	2 pcs \phi12	
11–20	450	-	-	14φ20	14φ20	-	-	2 pcs \$12	2 pcs \$12	
21-30	400	-	-	12φ20	12φ20	-	-	2 pcs \$12	2 pcs \$12	

Note: In the E-shaped shear wall configuration, the "long face" refers to the vertical spine of the "E", while the "short faces" correspond to the horizontal arms.

3.8.4. Coupling beam design

Since the building model has core shear walls in an E-shaped configuration, three coupling beams ertr defined on each story, as illustrated in blue in Fig. 7. If either of the conditions specified in Eq. 17 or Eq. 18 is met, the coupling beam shear rebars can be designed in the same manner as regular frame beams. Since the height of all coupling beams in the building model is 75 cm and the length is 200 cm, the condition specified in Eq. 17 is satisfied, and the shear rebar calculations for coupling beams were performed similarly to the regular frame beams. Table 19 presents the longitudinal rebar details for all coupling beams in the model. For all coupling beam sections, stirrup rebar was defined as $4\phi10/100$ in the confinement zone and $4\phi10/200$ in the span region.

$$l_n > 2h_k \tag{17}$$

$$V_d \le 1.5 b_w d f_{ctd} \tag{18}$$

3.9. The impact of local soil

Seismic performances of the structural elements were determined based on the elastic design spectra corresponding to ZB and ZC local soil classes. However, since the cross-sectional dimensions vary across certain floors (three different section areas for floors 1-3, 4-10, and 11-30) individual analyses were conducted for each of these floor groups, as discussed in the following subsections. The load combinations used in the analyses are presented in Table 20. Since different *R* and *D* coefficients were used in the analysis for the podium and tower parts, E1 and E2 loads were calculated separately for each part.

Table 19. Longitudinal rebar layout in coupling beams

C4	Top longitudinal rebar	— Web rebar
Story	Bottom longitudinal rebar	web rebar
1 – 3	$4\phi 18 + 2\phi 14$	2×2412 / 250
1 – 3	$4\phi 18 + 2\phi 14$	2×2φ12 / 250
4 – 10	$6\phi 22 + 3\phi 14$	2×2412 / 250
4 – 10	$6\phi 22 + 3\phi 14$	2×2φ12 / 250
11 – 15	$5\phi 22 + 3\phi 16$	2×2\phi12 / 250
11 – 13	$5\phi 22 + 3\phi 16$	2×2ψ12 / 230
16 - 20	$5\phi 22 + 2\phi 14$	2×2412 / 250
10 – 20	$5\phi 22 + 2\phi 14$	2×2φ12 / 250
21 – 25	$4\phi 22 + 2\phi 12$	2×2410 / 250
21 – 23	$4\phi 22 + 2\phi 12$	2×2φ10 / 250
26 – 30	$4\phi 18 + 3\phi 14$	2×2412 / 250
20 – 30	$4\phi 18 + 3\phi 14$	2×2φ12 / 250

Table 20. Load combinations

Story	Load combination	
1 – 3	G + Q + E1	
	G + Q + E2	
4 – 10	G + 0.95 Q + E1	
	G + 0.95 Q + E2	
11 – 30	G + 0.6 Q + E1	
	G + 0.6 Q + E2	

3.9.1. Comparison of column internal forces

The comparison of column internal forces for local soil classes ZB and ZC is presented in Fig. 9. The axial forces on the first floor were examined since the columns on this floor are the most critical columns belonging to the lowest floor (1-3) group. Floors 4, 11, and 21 were also evaluated due to the use of smaller column cross-sections at those levels. Additionally, in accordance with the TBEC-2018 [36] provisions, the axial force for each column was calculated considering two different load combinations.

Table 21 shows the axial load increases of the columns depending on the seismic load direction for the selected four floors.

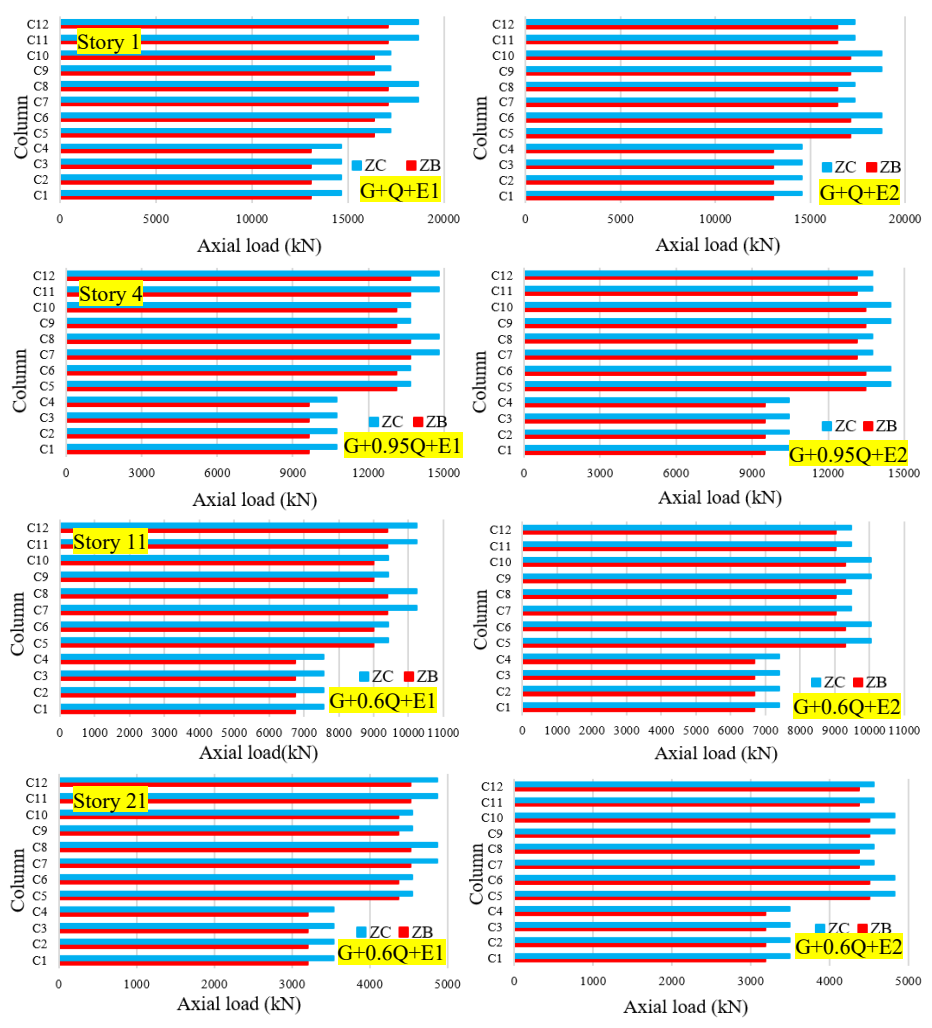


Fig. 9. Comparison of axial forces in columns

Table 21. Axial load increases in columns due to seismic effects

Floor	E1 (%)	E2 (%)
1	5 ~ 12	5 ~ 12
4	4 ~ 11	4 ~ 10
11	5 ~ 12	5 ~ 11
21	4 ~ 10	4 ~ 10

E1 and E2 represent load combinations defined in 3.9

3.9.2. Comparison of beam internal forces

The comparison of shear forces in frame and coupling beams for local soil classes ZB and ZC is presented in Figs. 10 and 11. As shown in the Figs., the beams were selected from the first floor as they represent the most critical elements in the lowest floor group (Floors 1-3). The beams on Floor 4 were selected as this level serves as the transfer floor. Beams on Floors 11 and 21 were also evaluated due to the use of smaller cross-sections at those levels. Furthermore, in accordance with the TBEC-2018 [36] provisions, shear force checks for each beam were carried out under two different load combinations.

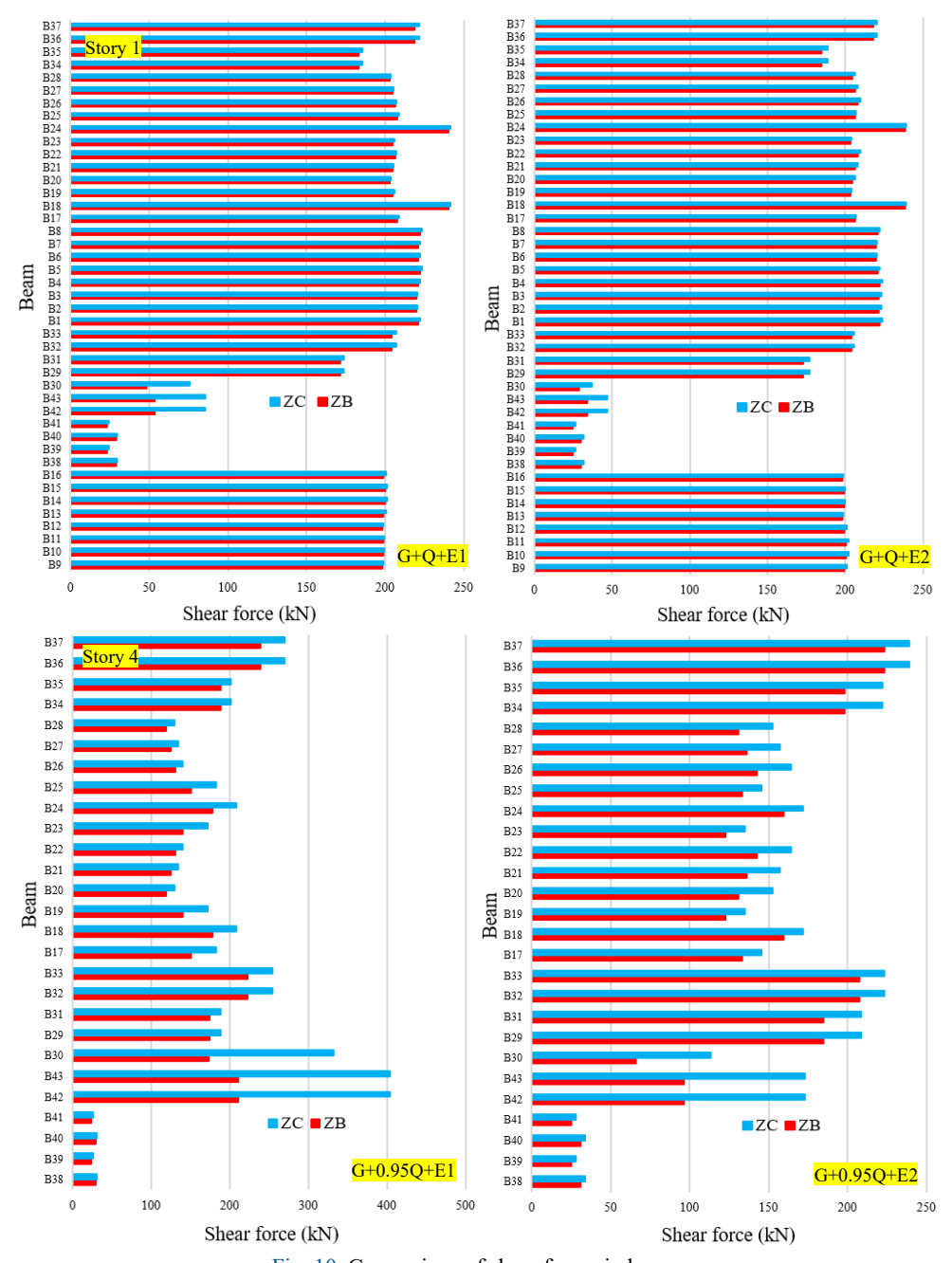


Fig. 10. Comparison of shear forces in beams

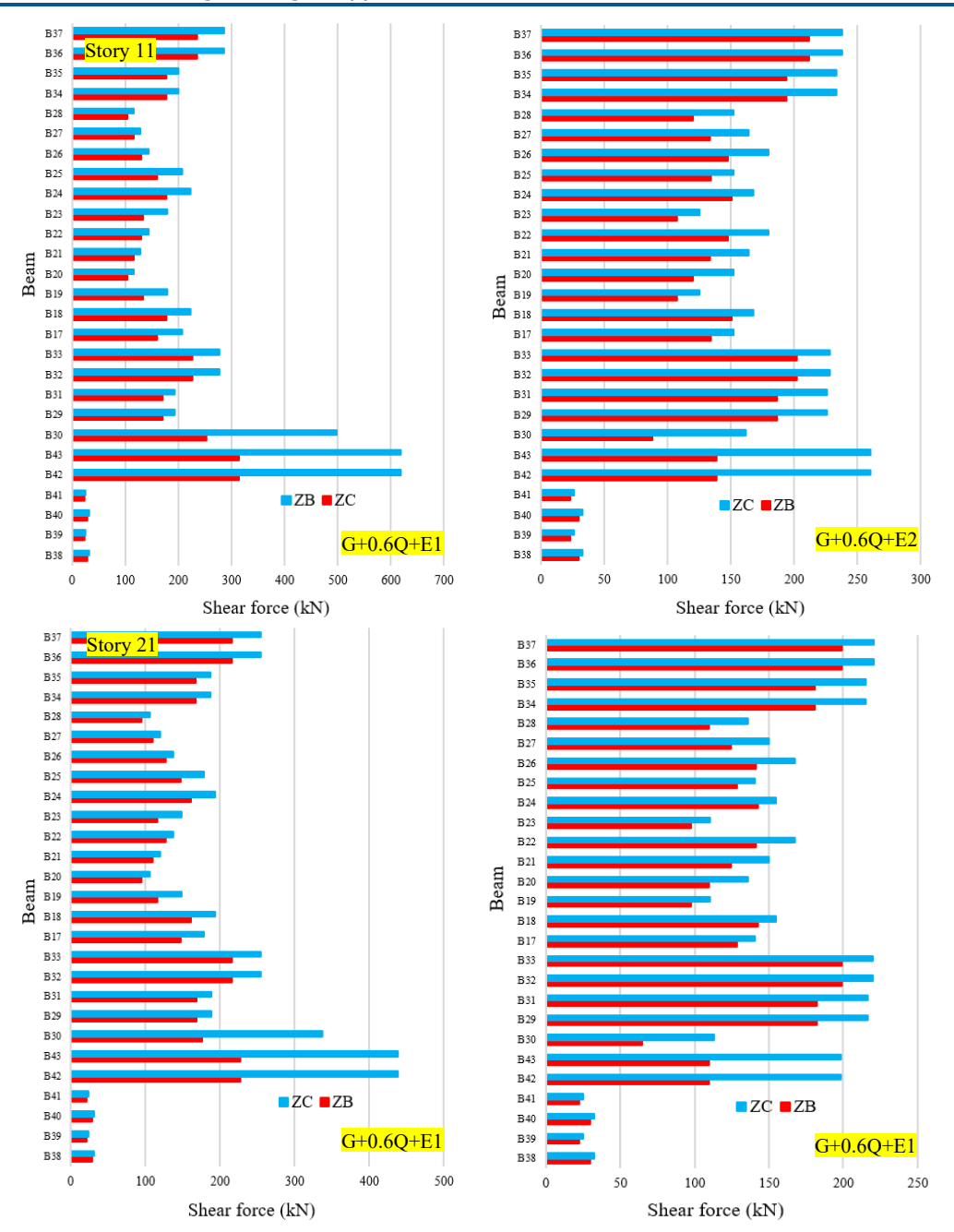


Fig. 11. Comparison of shear forces in beams

3.9.3. Comparison of internal forces in core shear walls

The comparison of flexural moments in the core walls for ZB and ZC local soil classes is shown in Fig. 12. The core walls on the first floor were selected because they are located on the lowest floor, and the core walls on the 4th floor were selected as they are on the transfer floor. The reason for evaluating the shear walls on the 11th and 21st floors is due to the smaller cross-sectional dimensions of the core walls at these levels. Additionally, under the TBEC-2018 [36] provisions, the moment capacity checks for core walls on each floor were performed under two load combinations.

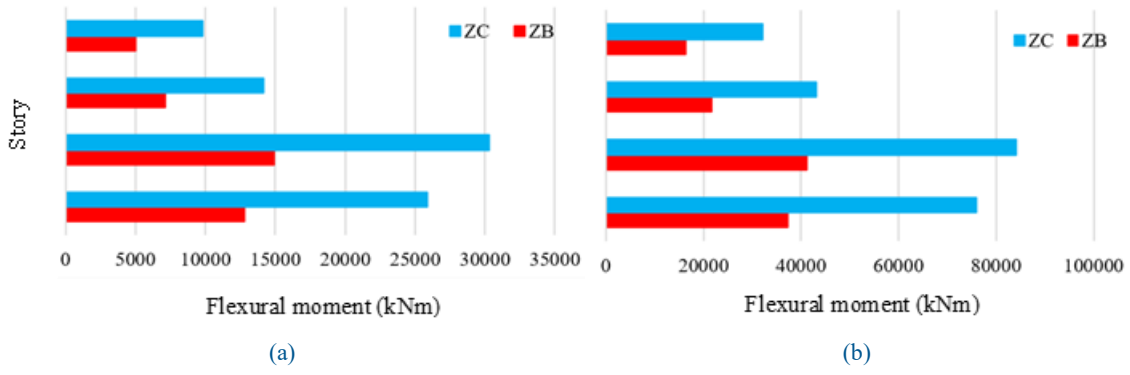


Fig. 12. Comparison of flexural moments for core shear walls: (a) E1, (b) E2

4. Conclusions

In this study, the modal response spectrum analysis was employed for the design and dimensioning of a 30-story symmetric-plan RC building model with core shear walls. The Controlled Damage (CD) performance level for the DD-2 earthquake ground motion was targeted based on the Strength-Based Design (SBD) principles. The conditions of TBEC-2018 [36] were taken into consideration in the modeling and analysis processes. In addition, to investigate the effect of local soil class on the seismic design of high-rise RC buildings, two different locations with ZB and ZC soil classes were selected, and the corresponding internal forces were obtained at the element level. The key findings obtained from the analysis are summarized below:

- Higher increases in axial loads were observed in corner columns (C1, C2, C3, and C4), independent of the seismic load direction, when transitioning from the ZB to ZC local soil class. These increases ranged from 10% to 12% across the floors.
- When transitioning from the ZB to ZC local soil class, the distribution of axial load increases in the
 interior columns, reversed with respect to seismic load direction. For example, in the E1 load
 combination, there was a 5% axial load increase in columns C5 and C6 on the first floor, while a 10%
 increase was observed under the E2 load combination.
- Regardless of the local soil class, the maximum axial load values were observed in the interior columns. However, in the selected floors, the maximum axial loads occurred in columns C7, C8, C11, and C12 under the E1 load combination, while maximum values were observed in columns C5, C6, C9, and C10 under the E2 combination.
- When transitioning from the ZB to ZC local soil class, the maximum increase in shear force across the selected floors was observed in the coupling beams (B42, B30, B43).
- When transitioning from the ZB to ZC local soil class, the maximum increase in shear force among the first-floor frame beams was observed in the elevator beams.
- When transitioning from the ZB to ZC local soil class, the earthquake-induced maximum increases in shear force at floors 4, 11, and 21 were observed in the exterior frame beams of the building.
- When transitioning from the ZB to ZC local soil class, the bending moments in the core shear walls at the selected floors approximately doubled, regardless of the earthquake direction.
- Regardless of the local soil class and earthquake direction, the maximum bending moments in the core shear walls were observed at Floor 4, which is the transfer floor.

In the symmetric-plan building model, the maximum axial load values were found in the interior columns, regardless of the local soil class. Therefore, the interior columns can be defined as the most critical columns. However, the maximum increases in the axial loads of the columns were observed at the corner columns, regardless of the earthquake direction. On the other hand, unlike the corner columns, the behavior of the

interior columns was directly dependent on the earthquake direction. This is why the decision regarding critical columns in high-rise buildings becomes more complex. For beams, it is an expected result that the maximum increase in shear force is observed in coupling beams. This is because coupling beams act as a protective element of the core shear wall system. In other words, they are designed to sustain damage during an earthquake to protect the core walls from taking damage. The obtained results indicate that the model was appropriately designed in this regard. Since the maximum shear force increases in beams were observed in the outer frame beams, it is recommended to strengthen these beams either by increasing their cross-sectional area or rebar ratio when the local soil class changes from better to poor. The impact of local soil class was mostly observed in the core wall system. This result indicates that more extensive strengthening may be required for the core walls when soil conditions deteriorate. Another critical part of the core wall system is the transfer floor. In buildings with podium floors, the transfer floor slabs, frame beams, coupling beams, and shear walls experience significant increases in internal forces. To mitigate these increases, the slab thickness at the transfer level can be designed to be higher.

In future studies aiming to investigate the effect of local soil on the seismic behavior of high-rise RC buildings, nonlinear time history analysis can be utilized. Additionally, parametric comparisons considering local soil differences under near-fault and far-fault ground motion scenarios with nonlinear analysis methods are planned. Examining near-fault effects requires the use of ground motion records. Moreover, both the literature and existing seismic codes typically define the near-fault zone as being within 10 km of a fault. However, this distance threshold may need to be reconsidered in cases of deteriorating soil conditions. When poor soil quality and near-fault effects are combined, the internal forces in structural elements can increase significantly. To explore this scenario further, the study could potentially include the ZD local soil class. For instance, in the case of ZD soil conditions, the near-fault threshold distance could reasonably be defined as greater than 10 km.

Future studies may also include parametric studies evaluating the effect of local soil for scenarios with and without consideration of soil-structure interaction. Regarding the effects of soil-structure interaction, excluding this interaction in the design of moderate-rise buildings leads to conservative (safe-side) results. However, in high-rise buildings, the opposite is true. Therefore, it is essential to account for soil-structure interaction in the design of high-rise buildings as an additional and critical factor. Since this subject primarily falls within the domain of geotechnical engineering, any modeling (full or partial representation of the soil) must be based on the assumptions and implications established in geotechnical literature.

Acknowledgments

This study is based on Kamran Samadi's master's thesis, titled "Performance-Based Seismic Design of High Rise Reinforced Concrete Buildings" supervised by Professor Baris Sayin and Assoc. Prof. Baris Gunes.

Conflict of interests

The author(s) declared no potential conflicts of interest with respect to the research, authorship, and/or publication of this article.

Funding

This research received no external funding.

Data availability statement

Data generated during the current study are available from the corresponding author upon reasonable request.

References

[1] Idhamou L, Mansouri M, Lakhouili A (2024) The assessment of the influence of soil type on the nonlinear seismic response of a corroded reinforced concrete portal frame. The Open Civil Engineering Journal 18: e18741495283898.

- [2] Dok G (2022) The effect of different soil classes on earthquake demands of reinforced concrete structures: Case study for Sakarya. Academic Platform Journal of Natural Hazards and Disaster Management 3(2):72–84.
- [3] Yassin A, Resatoglu R (2024) Nonlinear static analysis of RC buildings: Effects of soil type and seismic code differences on structural performance. Journal of Sustainable Architecture and Civil Engineering 3(36):111–129.
- [4] Navarro M, Vidal F, Enomoto T, Alcala FJ, Garcia-Jerez A, Sanchez FJ, Abeki N (2007) Analysis of the weightiness of site effects on reinforced concrete (RC) building seismic behaviour: The Adra town example (SE Spain). Earthquake Engineering and Structural Dynamics 36:1363–1383.
- [5] Tanijaya J, Kwandou R (2019) Strength evaluation of reinforced concrete structure for regular building due to earthquake load based on different soil types. Journal of the Civil Engineering Forum 5(2):123–129.
- [6] Elsadany SM, Fayed MN, Sorour TM, Anwar AM, Nasr NE (2024) Response reduction factor for structures with significant irregularities on different soil stratum. Civil Engineering Journal 10(3):757–778.
- [7] Zebua D, Wibowo LSB (2022) Effect of soil type on lateral displacement of reinforced concrete building. Applied Research on Civil Engineering and Environment 3(3):127–134.
- [8] Yön B, Öncü ME, Calayır Y (2015) Effects of seismic zones and site conditions on response of RC buildings. Građevinar 67(6):585–596.
- [9] Avcil F, Işık E, Büyüksaraç A (2022) The effect of local soil conditions on structure target displacements in different seismic zones. GUFBD / GUJS 12(4):1000–1011.
- [10] Ozmen HB, Tarakcı NC (2022) Effect of soil and foundation stiffness on the seismic behavior of mid-rise RC buildings. Research on Engineering Structures & Materials 8(2):385–402.
- [11] Jayalekshmi BR, Chinmayi HK (2016) Effect of soil stiffness on seismic response of reinforced concrete buildings with shear walls. Innovative Infrastructure Solutions 1(2).
- [12] Yön B, Calayır Y (2015) The soil effect on the seismic behaviour of reinforced concrete buildings. Earthquakes and Structures 8(1):133–152.
- [13] Dhakal S, Chaulagain H (2023) Seismic behaviour of plan irregular reinforced concrete buildings considering soil effects. Journal of Building Pathology and Rehabilitation 8(46).
- [14] Sivrikaya O, Türker E, Cüre E, Atmaca EE, Angin Z, Başağa HB, Altunişik AC (2025) Impact of soil conditions and seismic codes on collapsed structures during the 2023 Kahramanmaraş earthquakes: An in-depth study of 400 reinforced concrete buildings. Soil Dynamics and Earthquake Engineering 190:109119.
- [15] Lashgari A, Soghrat MR, Jafarian Y, Zafarani H (2024) The 2023 Turkey–Syria earthquake sequence: ground-motion and local site-effect analyses for Kahramanmaraş city. International Journal of Civil Engineering 22:877–899.
- [16] Kovrova VO, Volkova VE (2023) Analysis of the influence of different soil types on the natural frequencies of multi-storey reinforced concrete buildings. Strength of Materials and Theory of Structures 111:172–177.
- [17] Oz I, Senel SM, Palanci M, Kalkan A (2020) Effect of soil-structure interaction on the seismic response of existing low and mid-rise RC buildings. Applied Sciences 10:8357.
- [18] Balasudheer L, Patnaikuni CK, Kvgd B, Kumar BS (2017) Seismic analysis of R.C building with fixed and flexible base under different soil conditions. International Journal of Emerging Technologies in Engineering Research 5(10):41–49.
- [19] Hong JY, Ahmad SW, Adnan A, Muthusamy K, Ariffin NF, Yahaya FM, Mohsin SMS (2020) Seismic performance and cost analysis for reinforced concrete school building under different type of soil. Physics and Chemistry of the Earth 120:102933.
- [20] Wibowo LSB, Pradono MH, Fauzi HA, Sudarmadi S, Arman A, Perkasa M (2024) Seismic behavior for reinforced concrete buildings due to foundation settlement on different soil types. Iranian Journal of Science and Technology, Transactions of Civil Engineering 48:861–870.
- [21] İnce H, Toy E, Tolon M (2018) Influence of local soil conditions on the structural design and associated costs. International Journal of Engineering and Natural Sciences 1(1):21–25.

- [22] Işık E, Avcil F, Büyüksaraç A, Arkan E, Harirchian E (2025) Impact of local soil conditions on the seismic performance of reinforced concrete structures: In the context of the 2023 Kahramanmaraş earthquakes. Applied Sciences 15:2389.
- [23] Dogru M, Arslan G (2017) Seismic performance of an RC school building considering different soil classes. International Conference on Technology, Engineering and Science (ICONTES). Antalya, Turkey.
- [24] Orellana MA, Ruiz SE, Bojorquez J, Reyes-Salazar A, Bojorquez E (2021) Optimal load factors for earthquakeresistant design of buildings located at different types of soils. Journal of Building Engineering 34:102026.
- [25] Anand N, Mightraj C, Prince Arulraj G (2010) Seismic behaviour of RCC shear wall under different soil conditions. Indian Geotechnical Conference.
- [26] Jayalekshmi BR, Chinmayi HK (2013) Effect of soil flexibility on lateral natural period in RC framed buildings with shear wall. International Journal of Innovative Research in Science, Engineering and Technology 2(6):2067–2076.
- [27] Swamy BS, Prasad SK, Sunil N (2015) Influence of strong column & weak beam concept, soil type and seismic zone on seismic performance of RC frames from pushover analysis. International Journal of Research in Engineering and Technology 4(4):61–66.
- [28] Thusoo S, Modi K, Kumar R, Madahar H (2015) Response of buildings with soil-structure interaction with varying soil types. International Scholarly and Scientific Research & Innovation 9(4):414–418.
- [29] Raman RS, Rajitha A, K A, Deshmukh A, Kalra R, Maan P, AL-Attabi K (2024) Investigating three-dimensional RCC frames under seismic loading with various soil conditions. E3S Web of Conferences.
- [30] Choudhary N, Yadav BD, Mahato JK (2022) Comparative study of regular and irregular RC structure in different seismic zones and soil types. Earth & Environmental Science Research & Reviews 5(4):148–160.
- [31] Shelar VV, Pawar A, Shelar SV, Shingade VS, Kazi SM (2024) Impact of varying soil conditions on the design of tall building foundations. World Journal of Advanced Engineering Technology and Sciences 13(1):569–583.
- [32] Galal K, Naimi M (2008) Effect of soil conditions on the response of reinforced concrete tall structures to near-fault earthquakes. The Structural Design of Tall and Special Buildings 17:541–562.
- [33] Pahwa S, Prajapati D, Jain U (2017) A study of 30-storey dual system building with different soil conditions. International Journal of Engineering Research and Application 7(7, Part 1):29–34.
- [34] Hosseini M, Ramana Rao NV (2019) Impact of dynamic analysis of high-rise structure with dual system under different type of soil conditions, different type of RC shear wall & different load combination, load cases. Global Journal of Research in Engineering: (E) Civil and Structural Engineering 19(1):9–14.
- [35] ETABS (2018) Structural Analysis Program. Computers and Structures Inc., Berkeley, California.
- [36] TBEC (2018) Turkey Building Seismic Code: Rules for design of buildings under earthquake effect. Official Gazette, 18.03.2018, No. 30364 (in Turkish).
- [37] TS500 (2000) Requirements for Design and Construction of Reinforced Concrete Structures. Turkish Standards Institute, Ankara.
- [38] TS498 (1997) Design Loads for Buildings. Turkish Standards Institute, Ankara.
- [39] AFAD (2019) Turkey Earthquake Hazard Maps Interactive Web Application. Available at: https://tdth.afad.gov.tr/TDTH/main.xhtml
- [40] Özgül N (2011) Geology of Istanbul Province Area. Istanbul Metropolitan Municipality, Department of Earthquake Risk Management and Urban Development, İstanbul, Türkiye (in Turkish).
- [41] ASCE/SEI 7-22 (2022) Minimum Design Loads and Associated Criteria for Buildings and Other Structures. American Society of Civil Engineers. ISBN: 978-0-7844-8349-7.